

Periodic Coupled-Cluster Green's Function for Photoemission Spectra of Realistic Solids

Katelyn Laughon,¹ Jason M. Yu,² and Tianyu Zhu^{1,*}

¹Department of Chemistry, Yale University, New Haven, CT 06520

²Department of Chemistry, University of California, Irvine, Irvine, CA 92697

We present an efficient implementation of coupled-cluster Green's function (CCGF) method for simulating photoemission spectra of periodic systems. We formulate the periodic CCGF approach with Brillouin zone sampling in Gaussian basis at the coupled-cluster singles and doubles (CCSD) level. To enable CCGF calculations of realistic solids, we propose an active-space self-energy correction scheme by combining CCGF with cheaper many-body perturbation theory (*GW*) and implement the model order reduction (MOR) frequency interpolation technique. We find that the active-space self-energy correction and MOR techniques significantly reduce the computational cost of CCGF while maintaining the high accuracy. We apply the developed CCGF approaches to compute spectral properties and band structure of silicon (Si) and zinc oxide (ZnO) crystals using triple- ζ Gaussian basis and medium-size \mathbf{k} -point sampling, and find good agreement with experimental measurements.

Accurate first-principles simulation of spectral properties is key to understanding and designing solid-state materials for energy, catalysis, and quantum technologies. Density functional theory (DFT) [1] has been the workhorse for calculating band structure of solids due to its low cost, although it suffers from systematic errors and Kohn-Sham orbital energies do not formally describe the quasiparticle energies [2–4]. Correlated Green's function methods provide a formal route to computing photoemission spectra beyond DFT [5–12]. One of the most successful Green's function approaches for this task is the many-body perturbation theory, or *GW* [13–18]. Owing to proper treatment of dielectric screening, the *GW* theory in its one-shot formulation predicts accurate band gaps of weakly-correlated semiconductors and insulators. On the other hand, no *GW* formulation (e.g., self-consistency, DFT starting point, vertex correction) is known to be consistently reliable across weakly and strongly correlated materials. To achieve quantitative description of charged excitations beyond *GW*, one promising framework is the Green's function embedding such as dynamical mean-field theory (DMFT) [19–22] and self-energy embedding theory (SEET) [23, 24], but other approximations must be invoked, which require careful treatment.

Hence, it is necessary to develop higher-order *ab initio* Green's function methods for periodic systems. Recently, the coupled-cluster (CC) theory has been extended to compute ground-state and excited-state properties of realistic solids and shows great promise in simulating both weakly (e.g., silicon) and strongly (e.g., nickel oxide) correlated materials [25–29]. Meanwhile, molecular coupled-cluster Green's function (CCGF) implementations have been developed for studying photoelectron spectra of molecules and models [30–35] and solving impurity problems in *ab initio* DMFT calculations [21, 22, 36–38]. However, efficient periodic CCGF implementation capable of simulating photoemission spectra and band structure of realistic materials is not yet available due to high computational cost [39]. In this work, we fill this gap by developing accelerated periodic CCGF approach in Gaussian basis with Brillouin zone sampling.

We start with a description of molecular CCGF theory [32, 33, 36]. The one-particle Green's function of a given system $G(\omega) = G^+(\omega) + G^-(\omega)$ in frequency (energy) domain is defined as:

$$G_{pq}^+(\omega) = \langle \Psi_0 | a_p [\omega - (\hat{H} - E) + i\eta]^{-1} a_q^\dagger | \Psi_0 \rangle, \quad (1a)$$

$$G_{pq}^-(\omega) = \langle \Psi_0 | a_q^\dagger [\omega + (\hat{H} - E) - i\eta]^{-1} a_p | \Psi_0 \rangle, \quad (1b)$$

where $G^+(\omega)$ and $G^-(\omega)$ are addition (EA) and removal (IP) parts of Green's function, $|\Psi_0\rangle$ is the ground-state wave function, \hat{H} is the Hamiltonian, E is the ground-state energy, and η is a small broadening factor. a_p and a_q^\dagger are annihilation and creation operators on orbitals p and q . In coupled-cluster theory, the CC ground-state wave function is parameterized as

$$|\Psi_0\rangle = e^{\hat{T}} |\Phi_0\rangle, \quad (2)$$

with \hat{T} as the cluster excitation operator and $|\Phi_0\rangle$ as the Hartree-Fock determinant. In this work, we truncate the \hat{T} operator at the singles and doubles level (i.e., CCSD). The CC bra state is parameterized differently as:

$$\langle \Psi_0 | = \langle \Phi_0 | (1 + \hat{\Lambda}) e^{-\hat{T}}, \quad (3)$$

where $\hat{\Lambda}$ is the de-excitation operator. Inserting Eq. 2 and Eq. 3 into Eq. 1, one arrives at the CCGF equations:

$$G_{pq}^+(\omega) = \langle \Phi_0 | (1 + \hat{\Lambda}) \bar{a}_p [\omega - (\bar{H} - E) + i\eta]^{-1} \bar{a}_q^\dagger | \Phi_0 \rangle, \quad (4a)$$

$$G_{pq}^-(\omega) = \langle \Phi_0 | (1 + \hat{\Lambda}) \bar{a}_q^\dagger [\omega + (\bar{H} - E) - i\eta]^{-1} \bar{a}_p | \Phi_0 \rangle, \quad (4b)$$

where similarity transformed operators are defined as:

$$\begin{aligned} \bar{a}_p &= e^{-\hat{T}} \hat{a}_p e^{\hat{T}}, \\ \bar{a}_p^\dagger &= e^{-\hat{T}} \hat{a}_p^\dagger e^{\hat{T}}, \\ \bar{H} &= e^{-\hat{T}} \hat{H} e^{\hat{T}}. \end{aligned} \quad (5)$$

To efficiently solve Eq. 4, we define vectors $Y_q(\omega)$ and $X_p(\omega)$:

$$[\omega - (\bar{H} - E) + i\eta] Y_q(\omega) | \Phi_0 \rangle = \bar{a}_q^\dagger | \Phi_0 \rangle, \quad (6a)$$

$$[\omega + (\bar{H} - E) - i\eta] X_p(\omega) | \Phi_0 \rangle = \bar{a}_p | \Phi_0 \rangle, \quad (6b)$$

* tianyu.zhu@yale.edu

so that Eq. 4 becomes

$$G_{pq}^+(\omega) = \langle \Phi_0 | (1 + \hat{\Lambda}) \bar{a}_p Y_q(\omega) | \Phi_0 \rangle, \quad (7a)$$

$$G_{pq}^-(\omega) = \langle \Phi_0 | (1 + \hat{\Lambda}) \bar{a}_q^\dagger X_p(\omega) | \Phi_0 \rangle. \quad (7b)$$

To solve the set of linear equations in Eq. 6, $Y_q(\omega)$ and $X_p(\omega)$ are parameterized in the EOM-CCSD (equation-of-motion CCSD) approximation [40, 41]:

$$Y_q(\omega) = \sum_a y^a(q, \omega) a_a^\dagger + \sum_{i,a < b} y_i^{ab}(q, \omega) a_a^\dagger a_b^\dagger a_i, \quad (8a)$$

$$X_p(\omega) = \sum_i x_i(p, \omega) a_i + \sum_{i < j, a} x_{ij}^a(p, \omega) a_a^\dagger a_i a_j, \quad (8b)$$

where $Y_q(\omega)$ contains one-particle ($1p$) and two-particle one-hole ($2p1h$) terms and $X_p(\omega)$ contains $1h$ and $2h1p$ terms. We use the sparse linear equation solver GCROT(m,k) [42] as implemented in SciPy [43] to solve Eqs. 6 and 8.

For periodic systems, we work explicitly with \mathbf{k} -point (Brillouin zone) sampling in the reciprocal space. The \mathbf{k} -point

CCGF equation is

$$G_{pq}^+(\mathbf{k}, \omega) = \langle \Phi_0 | (1 + \hat{\Lambda}) \bar{a}_{p\mathbf{k}} [\omega - (\bar{H} - E) + i\eta]^{-1} \bar{a}_{q\mathbf{k}}^\dagger | \Phi_0 \rangle, \quad (9a)$$

$$G_{pq}^-(\mathbf{k}, \omega) = \langle \Phi_0 | (1 + \hat{\Lambda}) \bar{a}_{q\mathbf{k}}^\dagger [\omega + (\bar{H} - E) - i\eta]^{-1} \bar{a}_{p\mathbf{k}} | \Phi_0 \rangle. \quad (9b)$$

From the Green's function, one obtains momentum-dependent spectral function

$$A(\mathbf{k}, \omega) = -\frac{1}{\pi} \text{Im} G(\mathbf{k}, \omega), \quad (10)$$

whose trace defines density of states (DOS).

We implemented \mathbf{k} -point CCGF approach in PySCF quantum chemistry software package [44] using a hybrid MPI+OpenMP parallelization scheme. To avoid solving \mathbf{k} -point Λ equations, we approximate the Λ amplitudes as the complex conjugate of T amplitudes. We evaluated the accuracy of this approximation against an exact supercell (molecular) CCGF calculation on the diamond crystal and found excellent agreement (Fig. S1).

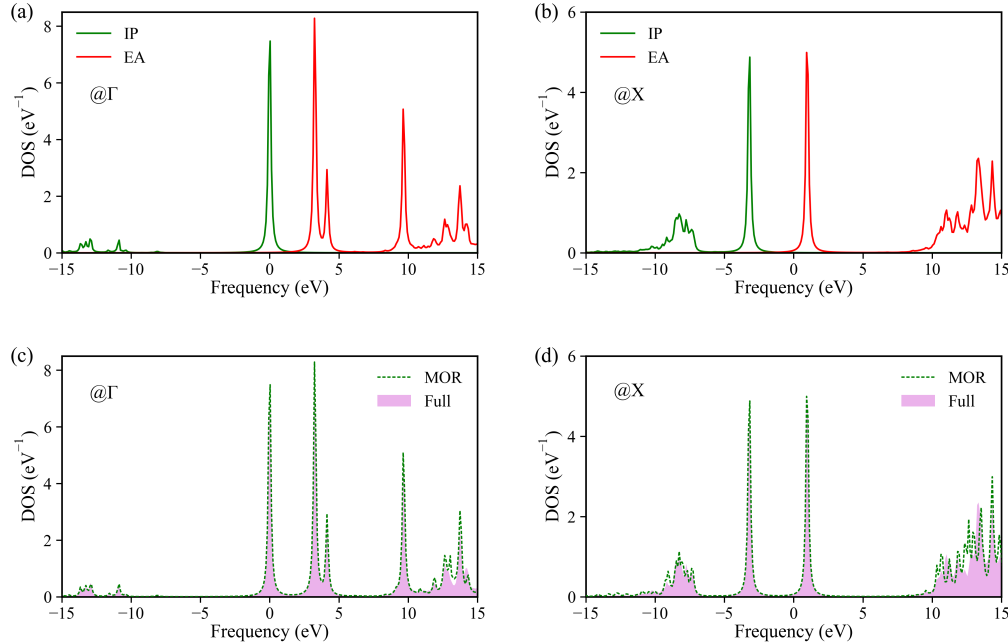


FIG. 1. Density of states of silicon crystal computed by periodic CCGF. GTH-DZVP basis set and $2 \times 2 \times 2$ \mathbf{k} -mesh were used. DOS is shifted so that valence band maximum (at Γ) is centered at 0 eV. A broadening factor of 0.1 eV is used. (a) DOS at Γ . (b) DOS at X. (c) MOR-CCGF against full CCGF at Γ . (d) MOR-CCGF against full CCGF at X.

In Fig. 1(a) and 1(b), we show momentum-dependent density of states (DOS) of Si computed by \mathbf{k} -point CCGF method with GTH-HF pseudopotential and GTH-DZVP basis set [45, 46] as well as $2 \times 2 \times 2$ \mathbf{k} -point sampling. Because our periodic CCGF approach is formulated on real-frequency axis, it is capable of computing photoemission spectra of valence, core, and high-virtual bands, which involve quasiparticle and satellite (e.g., [-15, -10] eV and [10, 15] eV in Fig. 1(a)) peaks.

Although it is now possible to perform small \mathbf{k} -point CCGF calculations, the high computational scaling of periodic CCGF prohibits its application to more complex materials. At each \mathbf{k} -point, frequency ω , and Green's function column/row (for EA/IP), the scaling of the EA part is $\mathcal{O}(N_{\mathbf{k}}^3 N_o N_v^4)$ and the scaling of the IP part is $\mathcal{O}(N_{\mathbf{k}}^3 N_o^3 N_v^2)$. $N_{\mathbf{k}}$, N_o , N_v are the number of sampled \mathbf{k} -points, occupied orbitals, and virtual orbitals (per unit cell, respectively). The overall cost for com-

puting $G^+(\mathbf{k}, \omega)$ and $G^-(\mathbf{k}, \omega)$ matrices for all \mathbf{k} -points are thus $\mathcal{O}(N_\omega N_{\mathbf{k}}^4 N N_o N_v^4)$ and $\mathcal{O}(N_\omega N_{\mathbf{k}}^4 N N_o^3 N_v^2)$, with $N = N_o + N_v$ and N_ω as the sampled frequency points. In the rest of this Letter, we describe acceleration techniques to reduce N_ω and N .

Model order reduction. To obtain high resolution in photoemission spectra, one usually needs to perform CCGF calculations on hundreds of frequency points. This large prefactor can be significantly lowered by the model order reduction (MOR) method, which is a technique for reducing computational complexity of mathematical models and has been successfully applied to compute X-ray absorption spectra and CCGF for molecules [34, 47]. We refer the readers to Ref. [34] for details of the MOR-CCGF implementation. Briefly speaking, in MOR-CCGF, one computes the full CCGF (Eq. 6) on a small set of selected frequency points (e.g., $N_\omega^{\text{MOR}} \approx 10-20$), then uses solved $X(\omega)$ or $Y(\omega)$ to construct a subspace. The original effective Hamiltonian (\tilde{H}) is then projected onto the subspace to form a much smaller model with dimension of $N_\omega^{\text{MOR}} \times N_\omega^{\text{MOR}}$. One finally solves CCGF equations on all N_ω frequency points ($N_\omega \approx 200-400$) using this reduced model, which has negligible cost. Thus, MOR is a frequency interpolation (sometimes extrapolation) technique that decreases the prefactor from N_ω to N_ω^{MOR} .

We implemented the MOR technique within our periodic CCGF code and tested the accuracy of MOR-CCGF on Si. In Fig. 1(c) and 1(d), we chose $N_\omega^{\text{MOR}} = 20$ (equally distributed on $[-15, 0]$ eV for IP and $[0, 15]$ eV for EA) and $N_\omega = 321$ respectively (meaning the cost of MOR-CCGF is 1/16 of full CCGF). MOR-CCGF reproduces the main quasiparticle peaks

around Fermi level perfectly compared to full CCGF calculations. Even the satellite peaks at $[-15, -5]$ eV and $[10, 15]$ eV are captured accurately. If one focuses only on the valence peaks, we found that $N_\omega^{\text{MOR}} = 8$ is enough to yield highly accurate CCGF DOS (see Fig. S2).

Active-space self-energy correction. Following the idea of frozen natural orbital coupled-cluster theory [48–50], we develop an active-space approach to reduce the number of orbitals in periodic CCGF calculations. Specifically, we show an efficient combination of CCGF and GW methods through a self-energy correction scheme.

We first perform a GW calculation on the system using Gaussian-based G_0W_0 method developed by one of the authors (T.Z.) [17]. Throughout this Letter, we employ the one-shot $G_0W_0@HF$ method that scales as $\mathcal{O}(N_{\mathbf{k}}^2 N^4)$. From the $G_0W_0@HF$ calculation, we obtain the GW density matrix $\gamma^{GW}(\mathbf{k}, \omega)$ using a linearized GW density matrix formalism [51] which guarantees conserving particle number. The GW density matrix is then diagonalized to derive a set of natural orbitals:

$$\gamma^{GW}(\mathbf{k})V(\mathbf{k}) = V(\mathbf{k})n(\mathbf{k}), \quad (11)$$

where $V(\mathbf{k})$ is the natural orbital (NO) coefficient and $n(\mathbf{k})$ is the occupation number of NOs. We then select M most partially occupied orbitals to form an active space and perform periodic CCGF calculation. Because $M < N$, the computational cost of CCGF is approximately decreased from $\mathcal{O}(N_\omega N_{\mathbf{k}}^4 N^6)$ to $\mathcal{O}(N_\omega N_{\mathbf{k}}^4 M^6)$. We note that we keep active space the same size for all \mathbf{k} -points to simplify the implementation.

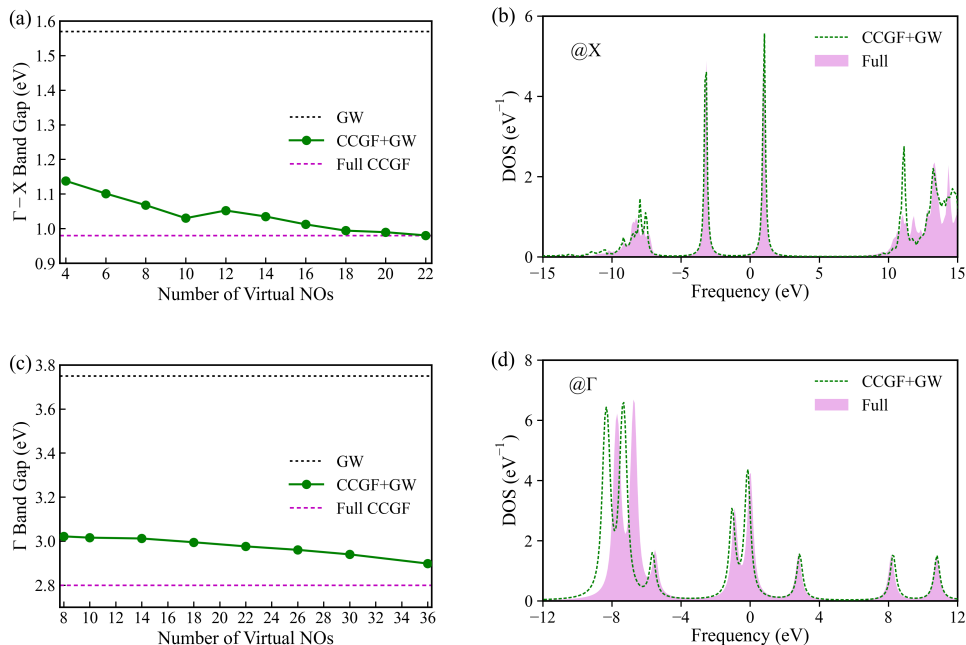


FIG. 2. Periodic CCGF results with active-space self-energy correction. (a) Γ -X band gap of Si computed by CCGF+ GW as a function of virtual NO number per unit cell. Full CCGF and $G_0W_0@HF$ results are also included. (b) DOS for Si at X computed by (8e, 14o) active-space CCGF+ GW and full CCGF. $\eta = 0.1$ eV. (c) Band gap of wurtzite ZnO computed by CCGF+ GW compared against full CCGF and $G_0W_0@HF$. MOR ($N_\omega^{\text{MOR}} = 8$) is employed for full CCGF and CCGF+ GW calculations. (d) DOS for ZnO at Γ computed by (16e, 18o) active-space CCGF+ GW and full CCGF. $\eta = 0.2$ eV.

However, this frozen natural orbital scheme does not work well for excited states and truncating the NO basis from N to M results in a loss of accuracy. To remedy the error, we define a self-energy correction term within the complete active space (CAS):

$$\Sigma_{\text{CAS}}(\mathbf{k}, \omega) = G_{\text{GW,CAS}}^{-1}(\mathbf{k}, \omega) - G_{\text{CC,CAS}}^{-1}(\mathbf{k}, \omega), \quad (12)$$

and transform it back to the full molecular orbital (MO) space

$$\Sigma_{\text{full}}(\mathbf{k}, \omega) = V(\mathbf{k})\Sigma_{\text{CAS}}(\mathbf{k}, \omega)V(\mathbf{k})^\dagger. \quad (13)$$

Then the CC+GW Green's function is computed through Dyson's equation:

$$G_{\text{CC+GW}}(\mathbf{k}, \omega) = [G_{\text{GW,full}}^{-1}(\mathbf{k}, \omega) - \Sigma_{\text{full}}(\mathbf{k}, \omega)]^{-1}, \quad (14)$$

where the GW Green's function ($G_{\text{GW,full}}$) for the full system is computed when deriving the natural orbital basis. We note that this scheme can also be applied using other low-level theories, such as MP2 or self-consistent GW [52, 53].

We benchmarked the accuracy of CCGF+GW on Si and wurtzite zinc oxide (ZnO). We used GTH-DZVP basis set and $2 \times 2 \times 2$ \mathbf{k} -point sampling for Si and def2-SV(P) basis set [54] and $2 \times 2 \times 1$ \mathbf{k} -point sampling for ZnO. In Fig. 2(a), we tested the Γ -X band gap of Si using different number of virtual NOs in the active space, while all (4) occupied orbitals are included. As a comparison, the full CCGF and G_0W_0 @HF band gaps are 0.98 eV and 1.57 eV, which correspond to 22 virtual orbitals per unit cell. As the number of active virtual NOs increases, the CCGF+GW band gap quickly converges to the full CCGF result. We find that using only 4 virtual NOs per unit cell, the CCGF+GW band gap is 1.14 eV, only 0.16 eV larger than full CCGF gap. At 10 virtual NOs, the CCGF+GW band gap error is only 0.05 eV (or 5%). We note that for DOS at Γ point, the CCGF+GW calculation with 10 virtual NOs takes 2 hours on 112 CPU cores, while the full CCGF calculation costs 19 hours using same resources.

The DOS for Si at X point is presented in Fig. 2(b) using an active space of (8e, 14o) (i.e., 8 electrons and 14 orbitals per unit cell). It is shown that not only the low-energy quasiparticle peaks are accurately described by CCGF+GW, but also the deeper valence and higher virtual spectra are well captured.

In Fig. 2(c) and 2(d), we present similar tests for ZnO. The full CCGF and G_0W_0 @HF band gap for ZnO are 2.80 eV and 3.75 eV, which correspond to 38 occupied and 38 virtual orbitals per unit cell. Fixing the number of active occupied orbitals to 8 in Fig. 2(c), reasonably accurate band gaps are produced by CCGF+GW. For example, at 10 virtual NOs, the CCGF+GW band gap is 3.02 eV and has 8% relative error compared to full CCGF. More test results on ZnO are available in the SI. The photoemission spectrum computed by (16e, 18o) CCGF+GW also shows good agreement with full CCGF in Fig. 2(d). The discrepancy in the [-10, -6] eV region is likely due to the small number of active occupied orbitals used in CCGF+GW.

Combining both active-space self-energy correction and MOR techniques, we study Si and ZnO using higher-quality basis set and larger Brillouin zone sampling. For Si, we used

the correlation-consistent GTH-cc-pVTZ basis set recently developed by Ye and Berkelbach [55] as well as GTH-HF pseudopotential. We applied MOR-CCGF+GW approach with an active space of (8e, 14o) per unit cell and $N_\omega^{\text{MOR}} = 8$. Using band interpolation technique based on intrinsic atomic orbital and projected atomic orbital (IAO+PAO) [39, 56, 57], we obtain band structure of Si from MOR-CCGF+GW calculation at $3 \times 3 \times 3$ \mathbf{k} -mesh in Fig. 3. We find that the CCGF band structure is in excellent agreement with experimental photoemission data [58].

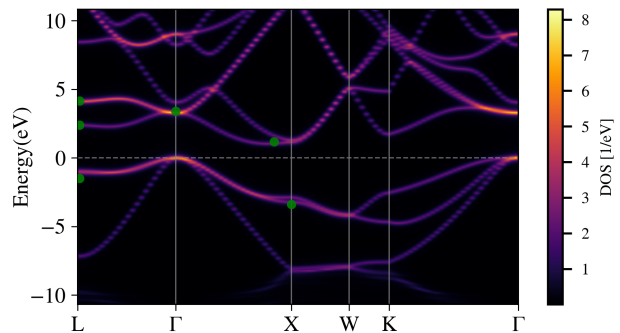


FIG. 3. Band structure of Si computed by MOR-CCGF+GW at $3 \times 3 \times 3$ \mathbf{k} -point sampling. Experimental data [58] are plotted in green circles.

To obtain Si band gap in the thermodynamic limit (TDL), we performed MOR-CCGF+GW calculations at $2 \times 2 \times 2$, $3 \times 3 \times 3$, and $4 \times 4 \times 4$ \mathbf{k} -meshes, and conducted a finite size extrapolation of band gap with respect to $N_{\mathbf{k}}^{-1/3}$. The results are summarized in Table I. Furthermore, we applied a correction term at $2 \times 2 \times 2$ \mathbf{k} -mesh that accounts for the error introduced by using small active space:

$$\Delta_{\text{CAS}} = E_g(L, 2 \times 2 \times 2) - E_g(2 \times 2 \times 2) \quad (15)$$

where $E_g(L, 2 \times 2 \times 2)$ corresponds to a (8e, 28o) MOR-CCGF+GW calculation and $E_g(2 \times 2 \times 2)$ refers to the (8e, 14o) calculation. The final estimated Si band gap is thus

$$E_g(\text{TDL} + \Delta_{\text{CAS}}) = E_g(\text{TDL}) + \Delta_{\text{CAS}}. \quad (16)$$

We find that $E_g(\text{TDL}) = 1.01$ eV and $\Delta_{\text{CAS}} = -0.03$ eV, leading to estimated CCGF band gap at 0.98 eV, which is 0.25 eV underestimated compared to the experimental band gap of 1.23 eV (taking zero-point renormalization effect into account). We note that our CCGF band gap is 0.21 eV smaller than EOM-CCSD result (1.19 eV) in Ref. [25], which is mainly caused by the use of different basis sets (GTH-cc-pVTZ vs. GTH-TZVP).

We then report MOR-CCGF+GW results on wurtzite ZnO, using an active space of (16e, 18o) per unit cell and $N_\omega^{\text{MOR}} = 8$. We employed cc-pVTZ-PP basis set and pseudopotential [59, 60] for Zn and cc-pVTZ basis set [61] for O. We present the DOS at Γ point with $4 \times 4 \times 3$ \mathbf{k} -point sampling in Fig. 4, since wurtzite ZnO has direct band gap at Γ . By plotting the orbital-resolved DOS, we find that the valence band

TABLE I. Band gaps (eV) of Si and wurtzite ZnO computed by MOR-CCGF+ GW at different k -point sampling. Finite size and CAS corrected (Extrap.+ Δ_{CAS}) band gaps are also included. Experimental values are taken from Ref. [18] and corrected for the zero-point renormalization effect.

	$2 \times 2 \times 2$	$3 \times 3 \times 3$	$4 \times 4 \times 4$	TDL+ Δ_{CAS}	Expt.
Si	0.78	0.85	0.89	0.98	1.23
	$2 \times 2 \times 1$	$3 \times 3 \times 2$	$4 \times 4 \times 3$	TDL+ Δ_{CAS}	Expt.
ZnO	2.39	3.47	3.97	4.94	3.60

maximum (VBM) of ZnO is mainly contributed from O-2 p orbitals, with minor character of Zn-3 d . On the other hand, the conduction band minimum (CBM) has dominant Zn-4 s and O-2 s components.

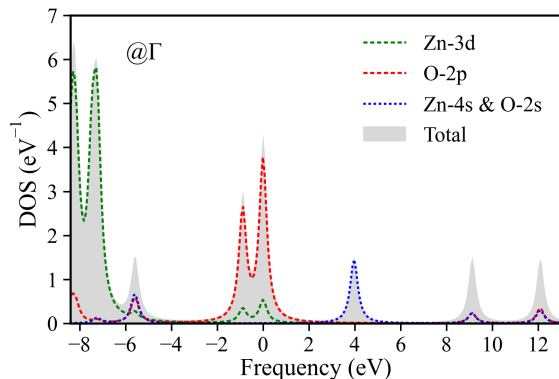


FIG. 4. Density of states of wurtzite ZnO at Γ point computed by MOR-CCGF+ GW with $4 \times 4 \times 3$ k -point sampling. $\eta = 0.2$ eV.

We also find that the MOR-CCGF+ GW band gap is 3.97 eV at $4 \times 4 \times 3$ k -mesh, only 0.37 eV larger than the experimental band gap of 3.60 eV. However, this good agreement is partially due to fortuitous error cancellation. The finite size

extrapolated band gap of ZnO from $2 \times 2 \times 1$, $3 \times 3 \times 2$, $4 \times 4 \times 3$ k -point calculations is 5.18 eV. The error from using small active space is estimated according to

$$\Delta_{\text{CAS}} = E_g(L, 2 \times 2 \times 1) - E_g(2 \times 2 \times 1), \quad (17)$$

where $E_g(L, 2 \times 2 \times 1)$ refers to a (52e, 76o) MOR-CCGF+ GW calculation and $E_g(2 \times 2 \times 1)$ is the (16e, 18o) calculation. Δ_{CAS} is computed to be -0.24 eV, thus our estimated CCGF band gap in the TDL is 4.94 eV, which is 1.34 eV overestimated than the experimental value. This study indicates CCGF at the EOM-CCSD level is not enough to produce quantitative accuracy in describing band gap of ZnO.

In conclusion, we developed efficient periodic coupled-cluster Green's function method and enabled simulating photoemission spectra of materials with high-quality basis set and realistic k -point sampling. We proposed and implemented active-space self-energy correction and MOR schemes, which significantly accelerate expensive periodic CCGF calculations. Periodic CCGF provides a higher-order Green's function tool than the commonly-used GW approximation, which is particularly attractive for benchmarking low-level theories and quantum embedding methods [22, 62] on spectral properties of solids.

Code availability. The periodic CCGF code and examples are available at <https://github.com/ZhuGroup-Yale/kccgf>.

ACKNOWLEDGMENTS

This work was supported by a start-up fund from Yale University. The National Science Foundation Graduate Research Fellowship Program (DGE-1745301) is acknowledged for support of J.M.Y. We thank Garnet Chan for helpful discussions and the Yale Center for Research Computing for supercomputing resources. This work also used the Extreme Science and Engineering Discovery Environment (XSEDE), which is supported by National Science Foundation grant number ACI-1548562.

-
- [1] W. Kohn and L. J. Sham, Self-consistent equations including exchange and correlation effects, *Phys. Rev.* **140**, A1133 (1965).
 - [2] J. P. Perdew, R. G. Parr, M. Levy, and J. L. Balduz, Density-functional theory for fractional particle number: Derivative discontinuities of the energy, *Phys. Rev. Lett.* **49**, 1691 (1982).
 - [3] J. P. Perdew and M. Levy, Physical content of the exact Kohn-Sham orbital energies: Band gaps and derivative discontinuities, *Phys. Rev. Lett.* **51**, 1884 (1983).
 - [4] J. P. Perdew, W. Yang, K. Burke, Z. Yang, E. K. Gross, M. Scheffler, G. E. Scuseria, T. M. Henderson, I. Y. Zhang, A. Ruzsinszky, H. Peng, J. Sun, E. Trushin, and A. Görling, Understanding band gaps of solids in generalized Kohn-Sham theory, *Proc. Natl. Acad. Sci. U. S. A.* **114**, 2801 (2017).
 - [5] L. Hedin, New method for calculating the one-particle Green's function with application to the electron-gas problem, *Phys. Rev.* **139**, A796 (1965).
 - [6] W. von Niessen, J. Schirmer, and L. S. Cederbaum, Computational methods for the one-particle green's function, *Comput. Phys. Reports* **1**, 57 (1984).
 - [7] B. Peng, N. P. Bauman, S. Gulania, and K. Kowalski, Coupled cluster Green's function: Past, present, and future, *Annu. Rep. Comput. Chem.* **17**, 23 (2021).
 - [8] S. Hirata, M. R. Hermes, J. Simons, and J. V. Ortiz, General-order many-body greens function method, *J. Chem. Theory Comput.* **11**, 1595 (2015).
 - [9] S. Hirata, A. E. Doran, P. J. Knowles, and J. V. Ortiz, One-particle many-body Green's function theory: Algebraic recursive definitions, linked-diagram theorem, irreducible-diagram theorem, and general-order algorithms, *J. Chem. Phys.* **147**, 44108 (2017).
 - [10] A. A. Rusakov and D. Zgid, Self-consistent second-order Green's function perturbation theory for periodic systems, *J. Chem. Phys.* **144**, 054106 (2016).
 - [11] S. Banerjee and A. Y. Sokolov, Third-order algebraic diagram-

- matic construction theory for electron attachment and ionization energies: Conventional and Green's function implementation, *J. Chem. Phys.* **151**, 224112 (2019).
- [12] O. J. Backhouse, A. Santana-Bonilla, and G. H. Booth, Scalable and Predictive Spectra of Correlated Molecules with Moment Truncated Iterated Perturbation Theory, *J. Phys. Chem. Lett.* **12**, 7650 (2021).
- [13] M. S. Hybertsen and S. G. Louie, Electron correlation in semiconductors and insulators: Band gaps and quasiparticle energies, *Phys. Rev. B* **34**, 5390 (1986).
- [14] D. Golze, M. Dvorak, and P. Rinke, The GW compendium: A practical guide to theoretical photoemission spectroscopy, *Front. Chem.* **7**, 377 (2019).
- [15] M. Shishkin and G. Kresse, Implementation and performance of the frequency-dependent GW method within the PAW framework, *Phys. Rev. B* **74**, 035101 (2006).
- [16] J. Deslippe, G. Samsonidze, D. A. Strubbe, M. Jain, M. L. Cohen, and S. G. Louie, BerkeleyGW: A massively parallel computer package for the calculation of the quasiparticle and optical properties of materials and nanostructures, *Comput. Phys. Commun.* **183**, 1269 (2012).
- [17] T. Zhu and G. K. L. Chan, All-Electron Gaussian-Based G_0W_0 for Valence and Core Excitation Energies of Periodic Systems, *J. Chem. Theory Comput.* **17**, 741 (2021).
- [18] X. Ren, F. Merz, H. Jiang, Y. Yao, M. Rampp, H. Lederer, V. Blum, and M. Scheffler, All-electron periodic G0W0 implementation with numerical atomic orbital basis functions: Algorithm and benchmarks, *Phys. Rev. Mater.* **5**, 13807 (2021).
- [19] A. Georges and G. Kotliar, Hubbard Model in Infinite Dimensions, *Phys. Rev. B* **45**, 6479 (1992).
- [20] G. Kotliar, S. Y. Savrasov, K. Haule, V. S. Oudovenko, O. Parcollet, and C. A. Marianetti, Electronic Structure Calculations with Dynamical Mean-Field Theory, *Rev. Mod. Phys.* **78**, 865 (2006).
- [21] T. Zhu, Z.-H. Cui, and G. K.-L. Chan, Efficient Formulation of Ab Initio Quantum Embedding in Periodic Systems: Dynamical Mean-Field Theory, *J. Chem. Theory Comput.* **16**, 141 (2020).
- [22] T. Zhu and G. K.-L. Chan, Ab initio full cell gw+dmft for correlated materials, *Phys. Rev. X* **11**, 021006 (2021).
- [23] A. A. Rusakov, S. Iskakov, L. N. Tran, and D. Zgid, Self-Energy Embedding Theory (SEET) for Periodic Systems, *J. Chem. Theory Comput.* **15**, 229 (2019).
- [24] S. Iskakov, C.-N. Yeh, E. Gull, and D. Zgid, *Ab Initio* Self-Energy Embedding for the Photoemission Spectra of NiO and MnO, *Phys. Rev. B* **102**, 085105 (2020).
- [25] J. McClain, Q. Sun, G. K.-L. Chan, and T. C. Berkelbach, Gaussian-based coupled-cluster theory for the ground-state and band structure of solids, *J. Chem. Theory Comput.* **13**, 1209 (2017).
- [26] T. Gruber, K. Liao, T. Tsatsoulis, F. Hummel, and A. Grüneis, Applying the coupled-cluster ansatz to solids and surfaces in the thermodynamic limit, *Phys. Rev. X* **8**, 021043 (2018).
- [27] Y. Gao, Q. Sun, J. M. Yu, M. Motta, J. McClain, A. F. White, A. J. Minnich, and G. K. L. Chan, Electronic Structure of Bulk Manganese Oxide and Nickel Oxide from Coupled Cluster Theory, *Phys. Rev. B* **101**, 165138 (2020).
- [28] X. Wang and T. C. Berkelbach, Excitons in Solids from Periodic Equation-of-Motion Coupled-Cluster Theory, *J. Chem. Theory Comput.* **16**, 3095 (2020).
- [29] A. Gallo, F. Hummel, A. Irmler, and A. Grüneis, A periodic equation-of-motion coupled-cluster implementation applied to F-centers in alkaline earth oxides, *J. Chem. Phys.* **154**, 064106 (2021).
- [30] M. Nooijen and J. G. Snijders, Coupled cluster approach to the single-particle Green's function, *Int. J. Quantum Chem.* **44**, 55 (1992).
- [31] M. Nooijen and J. G. Snijders, Coupled cluster Green's function method: Working equations and applications, *Int. J. Quantum Chem.* **48**, 15 (1993).
- [32] K. Bhaskaran-Nair, K. Kowalski, and W. A. Shelton, Coupled cluster Green function: Model involving single and double excitations, *J. Chem. Phys.* **144**, 144101 (2016).
- [33] B. Peng and K. Kowalski, Green's Function Coupled-Cluster Approach: Simulating Photoelectron Spectra for Realistic Molecular Systems, *J. Chem. Theory Comput.* **14**, 4335 (2018).
- [34] B. Peng, R. Van Beeumen, D. B. Williams-Young, K. Kowalski, and C. Yang, Approximate Green's Function Coupled Cluster Method Employing Effective Dimension Reduction, *J. Chem. Theory Comput.* **15**, 3185 (2019).
- [35] J. McClain, J. Lischner, T. Watson, D. A. Matthews, E. Ronca, S. G. Louie, T. C. Berkelbach, and G. K.-L. Chan, Spectral Functions of the Uniform Electron Gas via Coupled-Cluster Theory and Comparison to the GW and Related Approximations, *Phys. Rev. B* **93**, 235139 (2016).
- [36] T. Zhu, C. A. Jiménez-Hoyos, J. McClain, T. C. Berkelbach, and G. K.-L. Chan, Coupled-Cluster Impurity Solvers for Dynamical Mean-Field Theory, *Phys. Rev. B* **100**, 115154 (2019).
- [37] A. Shee and D. Zgid, Coupled Cluster as an Impurity Solver for Green's Function Embedding Methods, *J. Chem. Theory Comput.* **15**, 6010 (2019).
- [38] A. Shee, C. N. Yeh, and D. Zgid, Exploring Coupled Cluster Green's Function as a Method for Treating System and Environment in Green's Function Embedding Methods, *J. Chem. Theory Comput.* **18**, 664 (2022).
- [39] Y. Furukawa, T. Kosugi, H. Nishi, and Y. I. Matsushita, Band structures in coupled-cluster singles-and-doubles Green's function (GFCCSD), *J. Chem. Phys.* **148**, 204109 (2018).
- [40] J. F. Stanton and R. J. Bartlett, The equation of motion coupled-cluster method. A systematic biorthogonal approach to molecular excitation energies, transition probabilities, and excited state properties, *J. Chem. Phys.* **98**, 7029 (1993).
- [41] A. I. Krylov, Equation-of-Motion Coupled-Cluster Methods for Open-Shell and Electronically Excited Species: The Hitchhiker's Guide to Fock Space, *Annu. Rev. Phys. Chem.* **59**, 433 (2008).
- [42] E. de Sturler, Truncation Strategies for Optimal Krylov Subspace Methods, *SIAM J. Numer. Anal.* **36**, 864 (1999).
- [43] P. Virtanen, R. Gommers, T. E. Oliphant, M. Haberland, T. Reddy, D. Cournapeau, E. Burovski, P. Peterson, W. Weckesser, J. Bright, S. J. van der Walt, M. Brett, J. Wilson, K. J. Millman, N. Mayorov, A. R. J. Nelson, E. Jones, R. Kern, E. Larson, C. J. Carey, Í. Polat, Y. Feng, E. W. Moore, J. VanderPlas, D. Laxalde, J. Perktold, R. Cimrman, I. Henriksen, E. A. Quintero, C. R. Harris, A. M. Archibald, A. H. Ribeiro, F. Pedregosa, P. van Mulbregt, and SciPy 1.0 Contributors, SciPy 1.0: Fundamental Algorithms for Scientific Computing in Python, *Nat. Methods* **17**, 261 (2020).
- [44] Q. Sun, X. Zhang, S. Banerjee, P. Bao, M. Barbry, N. S. Blunt, N. A. Bogdanov, G. H. Booth, J. Chen, Z. H. Cui, J. J. Eriksen, Y. Gao, S. Guo, J. Hermann, M. R. Hermes, K. Koh, P. Koval, S. Lehtola, Z. Li, J. Liu, N. Mardirossian, J. D. McClain, M. Motta, B. Mussard, H. Q. Pham, A. Pulkin, W. Purwanto, P. J. Robinson, E. Ronca, E. R. Sayfutyarova, M. Scheurer, H. F. Schurkus, J. E. Smith, C. Sun, S. N. Sun, S. Upadhyay, L. K. Wagner, X. Wang, A. White, J. D. Whitfield, M. J. Williamson, S. Wouters, J. Yang, J. M. Yu, T. Zhu, T. C. Berkelbach, S. Sharma, A. Y. Sokolov, and G. K. L. Chan, Recent developments in the PySCF program package, *J. Chem. Phys.* **153**,

- 024109 (2020).
- [45] C. Hartwigsen, S. Goedecker, and J. Hutter, Relativistic Separable Dual-Space Gaussian Pseudopotentials from H to Rn, *Phys. Rev. B* **58**, 3641 (1998).
- [46] J. Vandevondele, M. Krack, F. Mohamed, M. Parrinello, T. Chassaing, and J. Hutter, Quickstep: Fast and Accurate Density Functional Calculations Using a Mixed Gaussian and Plane Waves Approach, *Comput. Phys. Commun.* **167**, 103 (2005).
- [47] R. Van Beeumen, D. B. Williams-Young, J. M. Kasper, C. Yang, E. G. Ng, and X. Li, Model Order Reduction Algorithm for Estimating the Absorption Spectrum, *J. Chem. Theory Comput.* **13**, 4950 (2017).
- [48] A. G. Taube and R. J. Bartlett, Frozen natural orbitals: Systematic basis set truncation for coupled-cluster theory, *Collect. Czechoslov. Chem. Commun.* **70**, 837 (2005).
- [49] A. G. Taube and R. J. Bartlett, Frozen natural orbital coupled-cluster theory: Forces and application to decomposition of nitroethane, *J. Chem. Phys.* **128**, 164101 (2008).
- [50] A. Landau, K. Khistyayev, S. Dolgikh, and A. I. Krylov, Frozen natural orbitals for ionized states within equation-of-motion coupled-cluster formalism, *J. Chem. Phys.* **132**, 014109 (2010).
- [51] F. Bruneval, Assessment of the Linearized GW Density Matrix for Molecules, *J. Chem. Theory Comput.* **15**, 4069 (2019).
- [52] M. Shishkin and G. Kresse, Self-consistent GW calculations for semiconductors and insulators, *Phys. Rev. B* **75**, 235102 (2007).
- [53] M. Van Schilfgaarde, T. Kotani, and S. Faleev, Quasiparticle self-consistent GW theory, *Phys. Rev. Lett.* **96**, 226402 (2006).
- [54] F. Weigend and R. Ahlrichs, Balanced basis sets of split valence, triple zeta valence and quadruple zeta valence quality for H to Rn: Design and assessment of accuracy, *Phys. Chem. Chem. Phys.* **7**, 3297 (2005).
- [55] H. Z. Ye and T. C. Berkelbach, Correlation-Consistent Gaussian Basis Sets for Solids Made Simple, *J. Chem. Theory Comput.* **18**, 1595 (2022).
- [56] G. Knizia, Intrinsic Atomic Orbitals: An Unbiased Bridge between Quantum Theory and Chemical Concepts, *J. Chem. Theory Comput.* **9**, 4834 (2013).
- [57] D. R. Hamann and D. Vanderbilt, Maximally localized Wannier functions for GW quasiparticles, *Phys. Rev. B* **79**, 045109 (2009).
- [58] T. Chiang, K. Frank, H. Freund, A. Goldmann, F. J. Himpsel, U. Karlsson, R. Leckey, and W. Schneider, *Electronic structure of solids: Photoemission spectra and related data*, Vol. 23A (Springer, Berlin, 1989).
- [59] D. Figgen, G. Rauhut, M. Dolg, and H. Stoll, Energy-consistent pseudopotentials for group 11 and 12 atoms: Adjustment to multi-configuration Dirac-Hartree-Fock data, *Chem. Phys.* **311**, 227 (2005).
- [60] K. A. Peterson and C. Puzzarini, Systematically convergent basis sets for transition metals. II. Pseudopotential-based correlation consistent basis sets for the group 11 (Cu, Ag, Au) and 12 (Zn, Cd, Hg) elements, *Theor. Chem. Acc.* **114**, 283 (2005).
- [61] T. H. Dunning, Gaussian basis sets for use in correlated molecular calculations. I. The atoms boron through neon and hydrogen, *J. Chem. Phys.* **90**, 1007 (1989).
- [62] Z. H. Cui, T. Zhu, and G. K.-L. Chan, Efficient Implementation of Ab Initio Quantum Embedding in Periodic Systems: Density Matrix Embedding Theory, *J. Chem. Theory Comput.* **16**, 119 (2020).
-

Supporting Information for: Periodic Coupled-Cluster Green's Function for Photoemission Spectra of Realistic Solids

I. VALIDATION OF \mathbf{k} -POINT CCGF CODE

We tested the \mathbf{k} -point CCGF implementation with Λ amplitudes approximated by complex conjugate of T amplitudes against a supercell (molecular) CCGF implementation without approximation on diamond crystal. We used $3 \times 1 \times 1$ \mathbf{k} -point sampling and GTH-DZVP basis sets. As shown in Fig. S1, \mathbf{k} -point CCGF DOS is in excellent agreement with supercell CCGF DOS.

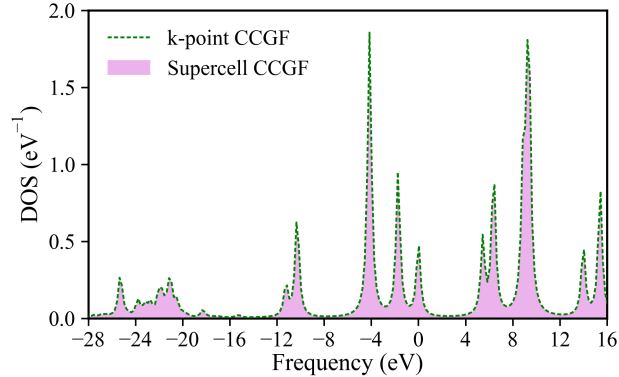


FIG. S1. Local DOS on diamond crystal computed by periodic CCGF. $\eta = 0.2$ eV.

II. MOR BENCHMARK

In addition to $N_{\omega}^{\text{MOR}} = 20$, we also tested different number of MOR frequency points for Si (GTH-DZVP basis and $2 \times 2 \times 2$ \mathbf{k} -mesh). As seen in Fig. S2, we find that $N_{\omega}^{\text{MOR}} = 8$ is sufficient to obtain highly accurate CCGF quasiparticle peaks around the Fermi level, although the accuracy in the deep valence and high virtual regions is sacrificed.

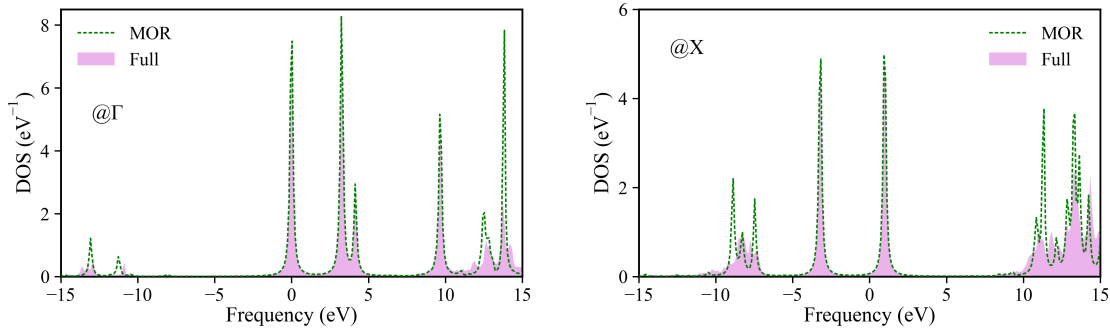


FIG. S2. DOS of Si computed by MOR-CCGF and full CCGF. $N_{\omega}^{\text{MOR}} = 8$ and $\eta = 0.1$ eV. Left: DOS at Γ . Right: DOS at X.

In Fig. S3, we show a test of MOR-CCGF on wurtzite ZnO using def2-SV(P) basis set and $2 \times 2 \times 1$ \mathbf{k} -point sampling. Again, we find $N_{\omega}^{\text{MOR}} = 8$ yields perfect agreement with full CCGF for low-energy quasiparticle peaks.

III. CCGF+GW TESTS ON ZNO

We performed detailed tests on the accuracy of active-space self-energy correction scheme on wurtzite ZnO using def2-SV(P) basis set and $2 \times 2 \times 1$ \mathbf{k} -mesh. Band gaps of ZnO from MOR-CCGF+GW calculations are summarized in Table S1. We find that by increasing the size of active space, CCGF+GW band gaps gradually approach the full CCGF value (i.e., 2.80 eV). In the meantime, one needs to use relative large active space, such as (36e, 36o) per unit cell, to reach under 5% relative error.

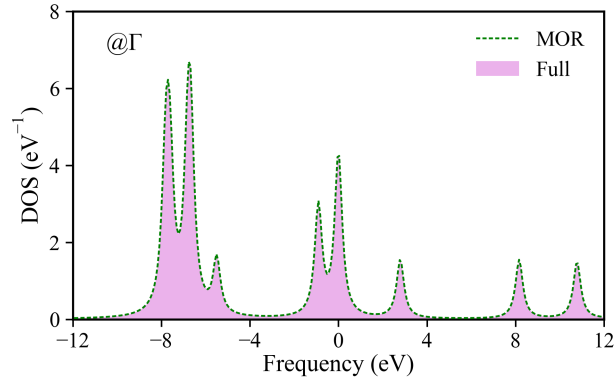


FIG. S3. DOS of wurtzite ZnO at Γ point computed by MOR-CCGF and full CCGF. $N_{\omega}^{\text{MOR}} = 8$ and $\eta = 0.2$ eV.

TABLE S1. Band gaps of wurtzite ZnO computed by MOR-CCGF+GW.

Active Space	Band Gap (eV)	Relative Error (%)
(16e, 18o)	3.02	7.8
(16e, 34o)	2.96	5.9
(20e, 20o)	3.01	7.8
(28e, 28o)	3.00	7.3
(36e, 36o)	2.92	4.3
(44e, 44o)	2.89	3.3
(52e, 52o)	2.88	2.9
(60e, 60o)	2.82	0.7
(76e, 76o)	2.80	0.0

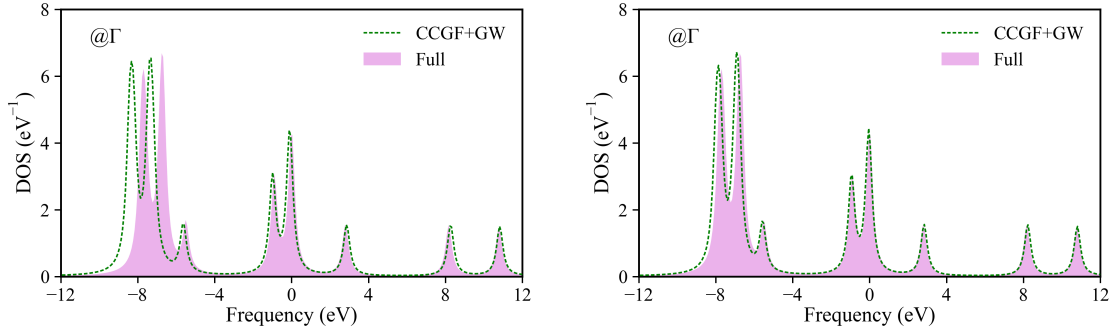


FIG. S4. DOS of ZnO at Γ point computed by MOR-CCGF+GW. $N_{\omega}^{\text{MOR}} = 8$ and $\eta = 0.2$ eV. Left: DOS using (16e, 34o) active space per unit cell. Right: DOS using (52e, 52o) active space per unit cell.

In Fig. S4, we show DOS of ZnO at Γ point computed by MOR-CCGF+GW at two different active spaces. We find that, compared to (16e, 18o) MOR-CCGF+GW calculation in Fig. 2(d), (16e, 34o) MOR-CCGF+GW only improves the description of low-energy bands slightly, while the discrepancy in the [-10, -6] eV region remains. When the active space is increased to (52e, 52o), we finally find good agreement with the full MOR-CCGF DOS over all frequency regions.